





Efficient polyethylene terephthalate degradation at moderate temperature: a protein engineering study of LC-cutinase highlights the key role of residue 243

Valentina Pirillo , Marco Orlando , Caren Battaglia, Loredano Pollegioni  and Gianluca Molla 

"The Protein Factory 2.0", Department of Biotechnology and Life Sciences (DBSV), University of Insubria, Varese, Italy

Keywords

green technology; improved LCC; polyethylene terephthalate biodegradation; rational design; structure-function relationships

Correspondence

G. Molla, "The Protein Factory 2.0", Department of Biotechnology and Life Sciences (DBSV), University of Insubria, Via J.H. Dunant 3, 21100 Varese, Italy
 Tel: +39 0332421414
 E-mail: gianluca.molla@uninsubria.it

Present address

Department of Biotechnology and Biosciences (BtBs), University of Milano-Bicocca, Piazza della Scienza 2, 20126, Milan, Italy

(Received 4 November 2022, revised 31 December 2022, accepted 23 January 2023)

doi:10.1111/febs.16736

Enzymatic degradation of poly(ethylene terephthalate) (PET) is becoming a reality because of the identification of novel PET-hydrolysing enzymes (PHEs) and the engineering of evolved enzyme variants. Here, improved variants of leaf-branch compost cutinase (LCC), a thermostable enzyme isolated by a metagenomic approach, were generated by a semi-rational protein engineering approach. Starting from a deleted LCC form lacking the secretion signal (Δ LCC), single and double variants possessing a higher activity on PET were isolated. The single-point F243T Δ LCC variant partially (~ 67%) depolymerized amorphous PET film producing ~ 21.9 mm of products after 27 h of reaction at 72 °C. The S101N/F243T Δ LCC double variant reached a further increase in activity on PET. Notably, for both single and double variants the highest conversion yield was obtained at 55 °C. Kinetics studies and molecular dynamics simulations support that a slight decreased affinity for PET is responsible for the superior degradation performance of the S101N/F243T variant and that this stems from a slightly higher flexibility of the active site region close to position 243. Furthermore, our findings question the need for a high reaction temperature for PET degradation, at least for LCC: at ≥ 70 °C, the conversion of amorphous PET into a more crystalline polymer, resistant to enzymatic hydrolysis, is favoured. The evolved S101N/F243T Δ LCC variant is able to depolymerize fully 1.3 g of untreated postconsumer PET waste in ≤ 3 days at 55 °C (using 1.25 mg of enzyme only), this making PET enzymatic degradation by engineering LCC a more ecofriendly and sustainable process.

Abbreviations

3PET, PET trimer monohydroxyethyl terephthalate 2-HE-(MHET)₃; BHET, bis(2-hydroxyethyl) terephthalate; CD, circular dichroism; CTAB, cetyltrimethylammonium bromide; DLS, dynamic light scattering; EG, ethylene glycol; GAFF, general Amber force field; IsPETase, *Ideonella sakaiensis* PETase; K_A , affinity constant; k_c , maximal rate of ester bond cleavage; LCC or LC-cutinase, leaf-branch compost cutinase; MD, molecular dynamics; MHET, mono(2-hydroxyethyl) terephthalate; PCR, polymerase chain reaction; PET, poly(ethylene terephthalate); PHE, PET-hydrolysing enzyme; PHL, polyester hydrolase Leipzig; *p*NPA, *p*-nitrophenyl acetate; μ EFED, per-residue effective free-energy decomposition; PSP or Phenol Red dye, phenolsulfonphthalein dye; RMSD, root-mean-square deviation; RMSF, root-mean-square fluctuation; SSM, site saturation mutagenesis; T_g , glass transition temperature; TIP3P, transferable intermolecular potential 3P; T_m , melting temperature; TPA, terephthalic acid; ΔG_{bind} , binding free energy; ΔH_{rel} , relaxation enthalpy; Δ LCC, truncated Δ LCC variant.

Introduction

It has been estimated that about 5.8 billion tonnes (~ 70% of the plastic materials produced worldwide since the early 1950s) have been disposed in dumpsites or into the natural environment [1]. This figure is likely to rapidly grow since, by 2050, more than 33 billion tons of plastics (mostly single use disposable packaging materials) will be globally produced. Importantly, plastics landfill did not decrease in the last 10 years [2]. This waste recalcitrant material adds up because of its poor biodegradability, posing several threats to the terrestrial and marine ecosystems and, eventually, to human's health [3,4] due to the accumulation of micro- and nanoplastics in the food chains [5,6]. Poly (ethylene terephthalate) (PET) is the most relevant polyester; it consists of alternating ethylene glycol (EG) and terephthalic acid (TPA) monomers linked by ester bonds. This thermoplastic polymer is widely used because of its excellent processing properties [7].

Within the context of plastics circular economy, a great interest has been attracted by the biocatalytic depolymerization of waste-derived PET that allows the production of the TPA and EG monomers for the resynthesis of novel PET possessing properties identical to the virgin PET and better than those of conventionally (mechanically or chemically) recycled PET [8]. Despite the polyester nature of PET, only few hydrolytic enzymes have been reported to catalyse its depolymerization [9]. In 2016, a PET hydrolytic enzyme (PHE) was identified from the mesophilic bacterium *Ideonella sakaiensis*, a microorganism that can completely degrade a small PET film within 42 days when cultivated in a fed-batch culture [10]. Later on, the two key enzymes involved in the hydrolysis of PET by *I. sakaiensis* were identified: an extracellular PET hydrolase (IsPETase) [11,12] able to cleave the PET polymers into the intermediates bis- and mono(2-hydroxyethyl) terephthalic acid (BHET and MHET respectively), and the cell membrane-associated MHET hydrolase [13].

The enzymatic susceptibility of PET is strictly related to its chemo-physical properties and, specifically, to the ratio between crystalline and amorphous fractions. Semi-crystalline PET shows a glass transition temperature (T_g) of ~ 70 °C. At this temperature, the mobile amorphous fraction of the PET polymer can be preferentially accessed by hydrolases and converted into soluble oligomeric and monomeric feedstocks [14]. This aspect encouraged the use of thermostable biocatalysts [15], produced by protein engineering [16–19] or identified by enzyme discovery approaches. For instance, LC-cutinase (LCC) isolated from a leaf-

branch compost, a thermophilic habitat for microbes, has an optimal temperature for PET hydrolysis of 50 °C [20,21]. Differently from IsPETase, fewer protein engineering studies were performed to improve the properties of LCC: the thermodynamics and kinetics of LCC aggregation were elucidated by [22], that also suggested glycosylation as a strategy to improve the solubility and stability of the enzyme at high temperatures. An improved LCC variant, carrying multiple substitutions, was described by [23]: this enzyme hydrolysed > 90% of postconsumer amorphized and micronized PET (after 10 h of incubation at 72 °C).

We recently reported on an efficient workflow for the *in vitro* evolution of PHEs, which employs a semi-rational protein engineering approach combined to a high-throughput colorimetric screening of variant libraries for their activity on PET nanoparticles [18]. This workflow was used to produce a variant of IsPETase, carrying four points mutations (TS- Δ IsPETase), able to depolymerize ~ 26% of PET microparticles and > 80% of PET nanoparticles at 45 °C. In the present study, and with the final aim to generate an efficient enzymatic tool for polyester degradation, the same workflow was applied to the evolution of a truncated version of LCC (Δ LCC) yielding the single (F243T) and the double (S101N/F243T) variants, which showed an increased activity on both PET microparticles and postconsumer PET at a moderate temperature (i.e. 55 °C).

Results

In silico analysis of the interaction between Δ LCC and PET

With the aim of identifying the residues of LCC that play a major role in the interaction with the substrate, thus being the most promising targets for generating libraries of single-point variants by site saturation mutagenesis (SSM), the interaction between the substrate PET and the protein was investigated through a computational analysis. A PET trimer of monohydroxyethyl terephthalate (2-HE-(MHET)₃, 3PET) was docked to Δ LCC (a deleted form of LCC lacking the 34 residue-long N-terminal secretion signal). Molecular dynamics (MD) simulations improved the best ligand–enzyme complex by allowing a reciprocal optimization of the active site side chains and PET interaction (Fig. 1A). In all three replicates, the substrate converged to a similar conformation after 100 ns of simulation supporting the reliability and stability of the predicted complex (Fig. S1). The overall (ΔG_{bind} , -35.4 ± 1.1 kcal·mol⁻¹) and per-residue binding free

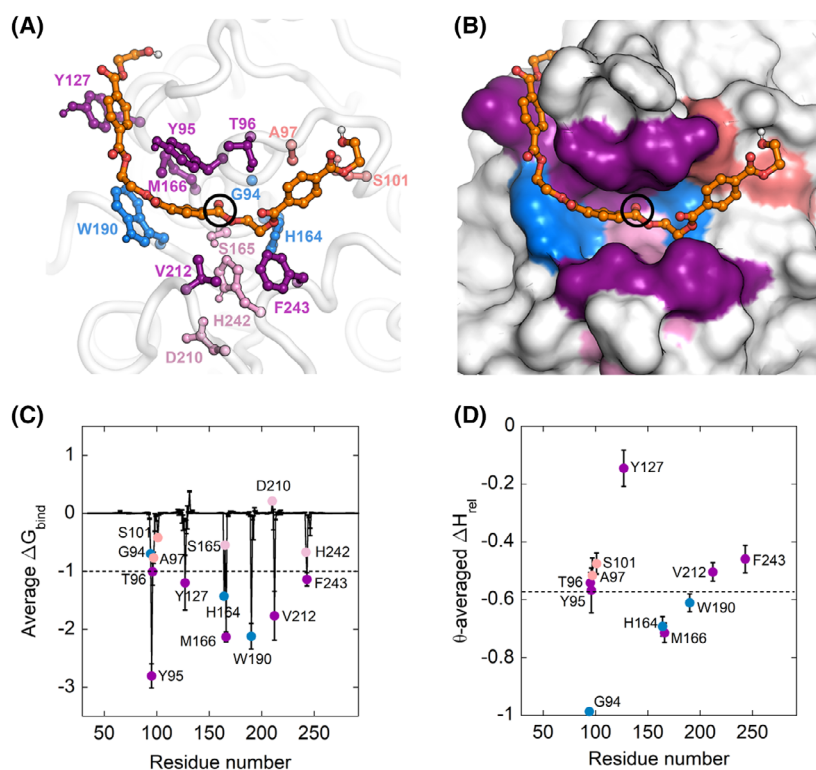


Fig. 1. Computational analysis of the interaction between Δ LCC and 3PET. (A, B) Representative frame of the MD simulation of the Δ LCC-3PET complex possessing the minimum estimated ΔG_{bind} . The ligand 3PET is represented as sticks and coloured according to the atom type (carbon in orange and oxygen in red): the carbon of the ester bond of the substrate which undergoes the nucleophilic attack is indicated by a black circle. Protein residues of the catalytic triad (light pink) involved in catalysis or 3PET interaction (for at least 30% of MD simulation frames) are visualized as balls and sticks; residues considered for the first or second round of SSM are depicted in purple or deep salmon respectively; the residues excluded from SSM are depicted in blue. Images were prepared with open-source PYMOL 2.5.0 (The PyMOL Molecular Graphics System, Version 2.5.0; Schrödinger, LLC, <https://github.com/schrodinger/pymol-open-source>). (C) Plot of average estimated per-residue ΔG_{bind} . The dashed line represents the ΔG_{bind} threshold of $-1 \text{ kcal}\cdot\text{mol}^{-1}$ used to predict hot-spot residues interacting with 3PET (Table S1). (D) Plot of θ -averaged Hamiltonian score difference with respect to the wild-type residue (ΔH_{rel}) for Δ LCC residues whose binding contribution is $\leq -1.0 \text{ kcal}\cdot\text{mol}^{-1}$. The dashed line represents the mean θ -averaged ΔH_{rel} of the whole sequence (-0.571). Symbols in panels (C, D) are coloured according to the colour scheme for panel A.

energy between the protein and the 3PET were estimated from MD simulations [24,25]. Specific residues contributing to the overall complex stability with an individual $\Delta G_{\text{bind}} \leq -1 \text{ kcal}\cdot\text{mol}^{-1}$ (i.e. Tyr95, Thr96, Tyr127, His164, Met166, Trp190, Val212, Phe243) were considered binding hot spots (Fig. 1C, Table 1).

In comparison to previously reported docking analyses between PHEs and PET, our model of the complex resembles the one reported by Sonnendecker (which docked a PET dimer of monohydroxyethyl terephthalate, 2-HE-(MHET)₂) while it significantly differs from the one reported by Tournier *et al.* based on a 3PET ligand [23,26]. Specifically, our results show a minor contribution of the residue Phe243 to the PET binding in comparison to the active site residues Tyr95, Tyr127 and Trp190 (Fig. 1A,B). It must be pointed out that

the use of a dimer of PET did not allow the investigation of the interaction between the third TPA ring and Phe243 (and surrounding residues).

The evolvability of each Δ LCC residue was predicted by calculating the probability of any possible mutation (expressed as a Hamiltonian score difference with respect to the wild-type residue, with more negative values being less probable) under a statistical Potts model of an alignment representative of the LCC family that accounts for inter-residue constraint positions. Tyr95, Thr96, Ala97, Ser101, Tyr127, Val212 and Phe243 possessed a Hamiltonian score averaged over all possible mutations > -0.571 (the score average over the whole sequence) and thus were predicted as promising candidates for SSM in the first round of mutagenesis (Fig. 1D). Positions Ala97 and Ser101 were excluded

Table 1. List of pairwise interactions between Δ LCC residues and the ligand 3PET observed during the MD simulations. The predicted average ΔG_{bind} contribution of each protein residue was calculated according to the MM-GBSA analysis. Only interactions at a distance ≤ 4.0 Å observed in $> 30\%$ of the MD frames are reported. The residues belonging to the catalytic triad are underlined.

Residue	Group	Type(s) of interaction	Frequency (% of MD frames)	ΔG_{bind} (kcal·mol ⁻¹)
Tyr95	Backbone; side chain	Hydrogen bond; Hydrophobic π -stacking	100.0	-2.81
<u>Ser165</u>	Side chain	Hydrogen bond	98.4	-0.55
Met166	Backbone	Hydrogen bond	98.7	-2.13
His164	Side chain	van der Waals	94.3	-1.43
Trp190	Side chain	Hydrophobic π -stacking	93.4	-2.12
Phe243	Backbone; side chain	Hydrophobic π -stacking	88.4	-1.14
Val212	Backbone; side chain	Hydrophobic contact	84.5	-1.77
Thr96	Side chain	Hydrogen bond	82.8	-1.01
<u>His242</u>	Side chain	van der Waals	80.2	-0.67
Ala97	Side chain	van der Waals	78.2	-0.77
Gly94	Backbone	van der Waals	68.0	-0.70
Tyr127	Side chain	Hydrophobic π -stacking	62.7	-1.20
Ser101	Backbone; side chain	Hydrogen bond	34.7	-0.42

from the first round of mutagenesis as they showed an individual $\Delta G_{\text{bind}} \leq -1$ kcal·mol⁻¹ (Fig. 1C).

Production of the first generation of evolved Δ LCC variants

Using the gene-encoding wild-type Δ LCC as template and NNK primers (to decrease the number of screened clones, Table S1), SSM at positions 95, 96, 127, 166, 212 and 243 was independently performed (Fig. S2). Position 166 was selected as a negative control since this position shows a high degree of conservation. Δ LCC libraries were screened for their activity on both BHET and PET nanoparticles (the substrate of main interest) using the Phenol Red dye (phenolsulfonphthalein dye, PSP) high-throughput colorimetric enzymatic assay at 540 nm on 96-well microtitre plates [18]. Variant libraries at position 95, 96, 127 and 166 showed a small fraction of clones possessing an improved enzymatic activity on PET nanoparticles in comparison to the wild-type Δ LCC (~ 8%, ~ 3%, ~ 9% and ~ 6% respectively, Table S2). This well matches with the high degree of conservation for Thr96, Tyr127 and Met166 in LCC homologues, as determined by evolutionary conservation analysis. However, position 95 shows a low evolutionary conservation degree (Table S2). As already observed in the case of IsPETase, the very low fraction of improved variants at this position could be related to its involvement in forming a hydrophobic cavity for substrate binding with Trp190 [18]. However, libraries generated at positions 212 and 243 showed a significant fraction of improved variants (~ 19% and ~ 23%, respectively, Table S2). Altogether, 14 Δ LCC variants

(namely, Y95H, Y95K, Y95R, T96A, T96H, T96Y, Y127P, Y127S, M166K, M166F, V212M, V212T, F243I and F243T) in the screening assay possessed a significantly increased activity in comparison to wild-type Δ LCC (from ~ 120% for the M166K variant to ~ 500% for the F243I one).

Biochemical properties of single-point Δ LCC variants

All selected variants were overexpressed and purified by metal-chelating affinity chromatography using the protocol optimized for the wild-type protein. All purified recombinant variants migrated as a single band at ~ 29 kDa and showed $> 90\%$ purity in SDS/PAGE. The substitutions affected the volumetric yield and the specific activity on *p*-nitrophenyl acetate (*p*NPA, a widely used small aromatic ester) and on PET nanoparticles (see *infra*) of the enzyme variants in comparison with the wild-type Δ LCC. The T96A and Y127P variants showed a volumetric yield similar to the wild-type; variants Y95H, Y95K, Y95R, M166K, V212T and F243I showed an improved volumetric yield (from 140% to 164%) while a lower figure was apparent for the T96H, T96Y, Y127S, M166F, V212M and F243T variants (from 36% to 52%, Table S3). Interestingly, the variants at position 127 and 212, sites showing a low degree of conservation, possessed a significantly increased specific activity on *p*NPA (Fig. 2).

The activity of the selected Δ LCC variants was investigated on PET nanoparticles using the turbidimetric assay at 50 °C. When a fixed concentration of PET nanoparticles (~ 96 $\mu\text{g}\cdot\text{mL}^{-1}$, mean diameter of

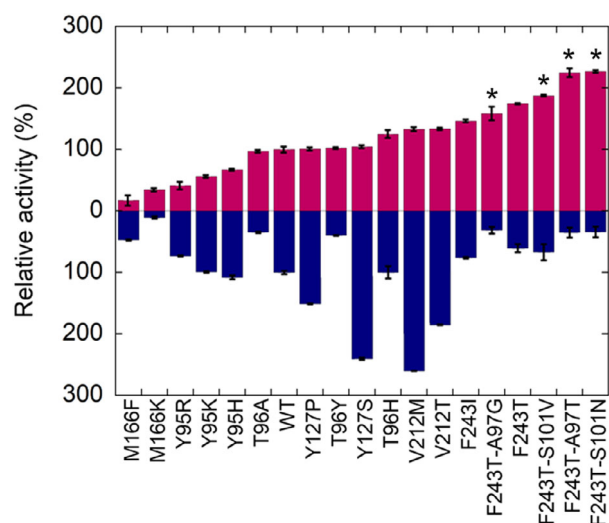


Fig. 2. Relative activity of Δ LCC variants ($0.02 \text{ mg}\cdot\text{mL}^{-1}$) on PET nanoparticles (red) and on *p*NPA (blue). The activity of the wild-type enzyme is set as 100%. Error bars indicate the standard deviation ($n = 3$). Reaction conditions: $0.094 \text{ mg}\cdot\text{mL}^{-1}$ of nanoparticles at 50°C or 1 mM *p*NPA at 30°C in 50 mM Tris-HCl buffer, 100 mM NaCl, pH 8.0. *Second-generation variants.

$\sim 80 \text{ nm}$) was incubated with $20 \mu\text{g}\cdot\text{mL}^{-1}$ of Δ LCC variants, a linear decrease in the $\text{OD}_{600 \text{ nm}}$ signal was observed after an equilibration phase of $\sim 1 \text{ min}$. An enzyme saturating condition was used, that is, a concentration of the enzyme at which the measured activity was not affected by the ratio between the PET nanoparticles and the enzyme [27]. Compared to wild-type Δ LCC, the F243T variant showed the largest increase in activity on PET nanoparticles (175%), followed by the F243I (151%), V212T (134%), V212M (133%) and T96H (125%) variants. Interestingly, no correlation between increased activity on PET nanoparticles at 50°C and on *p*NPA at 30°C was apparent; for example, the Δ LCC variants at position 243 (one of the most active on PET nanoparticles) showed a decreased activity on *p*NPA (Fig. 2, Table S3). We propose that substitutions increasing the PET hydrolytic activity (i.e. F243T) are often detrimental for the general esterase activity of Δ LCC, probably because of the altered geometry of the relevant active site residues required for binding and orientation of such as different substrates.

Biodegradation of different PET samples by single-point Δ LCC variants: the effect of temperature

The polymer degradation by the single-point Δ LCC variant at each position showing the highest activity

on PET nanoparticles was now investigated on different PET samples (variants at positions 95 and 166, which produced only poorly effective enzymes, were excluded).

At first, purified wild-type, T96H, Y127P, V212T or F243T Δ LCC ($40 \mu\text{g}$ each) were added to 1 mL of reaction mixture containing an amorphous PET film swatch of 7 mg (the reference substrate for the characterization of PHEs) and were incubated at 72°C for 68 h (i.e. the optimal reaction temperature for the PET hydrolysis as reported by Tournier *et al.*) [23] (Fig. 3A). The degradation kinetics was followed by monitoring the increase of the absorbance at 240 nm of the reaction supernatant due to the accumulation of the soluble aromatic compounds BHET, MHET and TPA deriving from PET degradation [18,27]. After 27 h of incubation, the biodegradation of PET film by the F243T variant was over with a production of 21.9 mM of products (conversion yield of $\sim 61\%$). This corresponds to a reaction rate of $0.48 \text{ mmol}_{\text{products}}\cdot\text{mg}_{\text{enzyme}}^{-1}\cdot\text{day}^{-1}$, a value ~ 1.2 -fold higher than with wild-type Δ LCC that, in the same time interval, produced 17.4 mM products. The Y127P variant showed a kinetics similar to the wild-type enzyme, while the T96H and V212T variants showed very poor PET depolymerization. In all cases, the final product concentration was lower than the maximal theoretical one (36.1 mM), even for the F243T variant (Table 2). A further addition of $40 \mu\text{g}$ of F243T variant did not significantly increase the concentration of PET depolymerization products (data not shown). This result suggests that the end of the reaction was not due to enzyme full inactivation but it could be related to an alteration in the physical properties of the PET substrate at 72°C , resulting in a partial crystallization of the polymer, as already observed by [23,28].

Next, in order to evaluate the activity of Δ LCC variants on a substrate resembling the postconsumer PET (i.e. a PET with a crystallinity fraction up to 33.8% [17]), a depolymerization reaction was setup using a high crystallinity PET microplastics (diameter $300 \mu\text{m}$). Purified variants were added to 1 mL of reaction mixture containing 40 mg PET microparticles and were incubated at 72°C . Notably, the reaction was over after 2 h of incubation; only a marginal amount ($2\text{--}7\%$) of reaction products was generated during the subsequent 1.5 h of incubation (Fig. 3B). The best variant (F243T Δ LCC) generated 23.2 mM soluble products after 2 h with a productivity rate of $7.0 \text{ mmol}_{\text{products}}\cdot\text{mg}_{\text{enzyme}}^{-1}\cdot\text{day}^{-1}$ and a 11.1% conversion yield of PET microparticles (Table 2). Interestingly, the presence of PET microparticles increased the

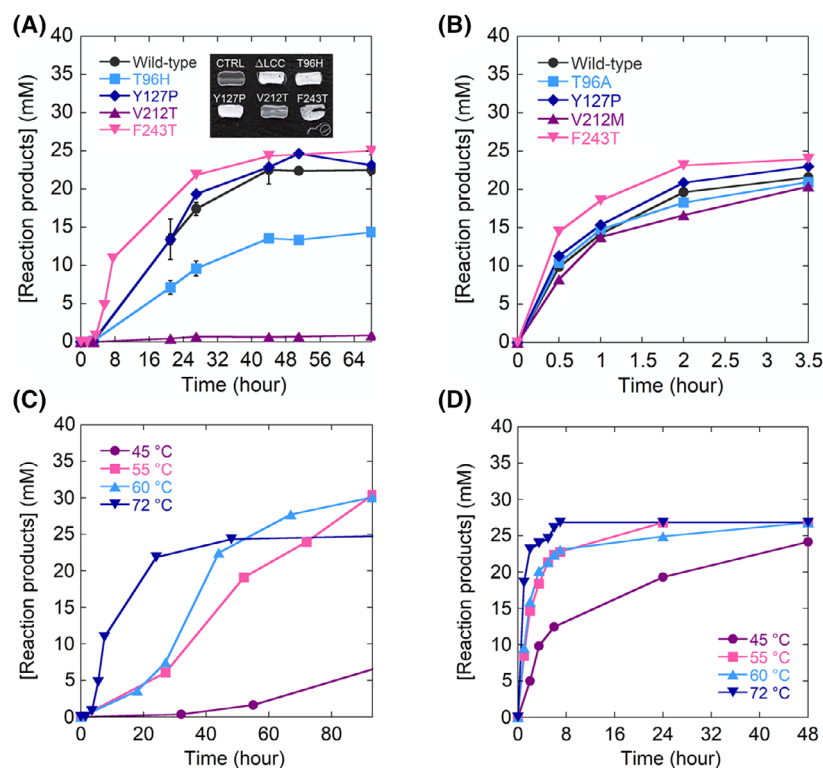


Fig. 3. Biodegradation of different PET types catalysed by Δ LCC variants at different temperatures. (A) Biodegradation of 7 mg·mL⁻¹ of amorphous PET film by different Δ LCC variants. Inset, photograph shows the residual PET film after incubation with the enzyme at 72 °C for 68 h. (B) Biodegradation of 40 mg·mL⁻¹ PET microplastics at 72 °C by different Δ LCC variants. Panel (A) and (B): wild-type (●), T96H (■), Y127P (◆), V212T (▲) and F243T (▼) Δ LCC. Reaction conditions: 0.04 mg·mL⁻¹ of Δ LCC variants in 100 mM potassium phosphate buffer, pH 8.0. (C, D) Biodegradation of amorphous PET film (C) and PET microparticles (D) at different temperatures by the F243T variant: 45 °C (●), 55 °C (■), 60 °C (▲) and 72 °C (▼). Reaction conditions as in panels A and B. In all cases, the reaction time course was followed through the determination of the total amount of soluble reaction products in the supernatant of the reaction mixture. Error bars indicate the standard deviation ($n = 3$).

rate of inactivation of the biocatalysts: the residual activity of the enzymes was < 25% after only 0.5 h of incubation (data not shown). It is plausible that the decrease in soluble active enzyme arises from its adsorption onto the surface of the PET microparticles, as already observed for IsPETase [18,29].

With the aim to prevent the crystallization of the amorphous PET film and to prevent the thermal inactivation of the biocatalyst, the temperature of the depolymerization reactions was decreased below 65 °C (i.e. below the T_g for amorphous PET). Under these conditions, the depolymerization yield increased even if the initial productivity rates were lower than the reaction performed at 72 °C. The F243T variant reached a ~ 84% product yield at 55–60 °C (Fig. 3C); the highest productivity rates were 0.22 mmol_{products}·mg_{enzyme}⁻¹·day⁻¹ (at 52 h) and 0.31 mmol_{products}·mg_{enzyme}⁻¹·day⁻¹ (at 44 h) at 55 °C and at 60 °C respectively. A similar product yield (81%) was obtained following the incubation at 45 °C, but the reaction completion required almost 16 days (Fig. S3). Interestingly, at this temperature the residual activity at the end of the reaction was still 60% for the F243T variant, while values of 70% and 53% were observed at 55 °C and 60 °C, respectively, after 4 days of incubation. However, no significant differences in the

depolymerization yield were observed when PET microparticles were incubated with the F243T variant at different temperatures (Fig. 3D).

Second generation of evolved Δ LCC variants

Since the two most improved Δ LCC variants were obtained by introducing substitutions at position 243, this region of the active site was further inspected. Two small residues, namely Ala97 and Ser101, are close to the substrate on the opposite side of the active site cleft (Fig. 1A). These residues, corresponding to residues Ala65 and Ser69 in polyester hydrolase PHL7, were predicted by our analysis and by [26] to play a minor contribution to the overall binding energy of the enzyme–PET complex and to be prone to accept substitutions (Fig. 1C). Δ LCC double variant libraries at these two positions were generated by SSM using the F243T variant as the starting sequence (Table S1). Interestingly, the library of variants at position 97 showed a high fraction of clones with an increased activity on BHET and PET substrates (~ 24% and ~ 18% respectively); while, the fraction of most active variants at position 101 was significantly lower (~ 8% with both substrates, Table S2). Four double variants (namely A97G/F243T, A97T/F243T, S101N/F243T

Table 2. Comparison of the depolymerization performances of selected Δ LCC variants on amorphous PET film, postconsumer PET waste and PET microparticles at 45 °C, 55 °C, 60 °C, or 72 °C. The full depolymerization of 7 mg of PET film in 1 mL of reaction mixture film corresponds to the generation of 36.4 mm of soluble products and of 40 mg of microPET to 208 mm of soluble products.

Δ LCC variant	Temperature (°C)	[E] (μ g)	Time (h)	[Products] (mm)	Product rate formation ($\text{mmol}_{\text{products}} \cdot \text{mg}_{\text{enzyme}}^{-1} \cdot \text{day}^{-1}$)	Depolymerization yield (%)
Amorphous PET film						
Wild-type	72	40	27 (44)	17.4 (22.5)	0.39 (0.31)	48 (62)
T96H	72	40	27 (44)	9.6 (13.6)	0.21 (0.18)	26 (37)
Y127P	72	40	27 (44)	19.4 (22.8)	0.43 (0.31)	53 (63)
V212T	72	40	27 (44)	0.7 (0.6)	0.02 (0.01)	2 (2)
F243T	72	40	27 (44)	21.9 (24.3)	0.48 (0.33)	60 (67)
Wild-type	60	40	39 (63)	6.3 (15.9)	0.10 (0.15)	17.4 (44.0)
F243T	60	40	39 (63)	15.2 ^a (27.7) ^b	0.23 (0.26)	42.1 (76.7)
A97T/F243T	60	40	39 (63)	10.2 (29.0)	0.16 (0.28)	28.3 (80.3)
S101N/F243T	60	40	39 (63)	22.1 (30.4)	0.34 (0.29)	60.5 (83.5)
Wild-type	55	40	65 (89)	16.5 (23.1)	0.15 (0.16)	46 (64)
F243T	55	40	65 (89)	24.8 (32.3)	0.23 (0.22)	68 (89)
A97T/F243T	55	40	65 (89)	22.8 (27.6)	0.21 (0.19)	63 (76)
S101N/F243T	55	40	65 (89)	33.1 (33.3)	0.31 (0.22)	91 (91)
Wild-type	55	5	42 (90)	15.8 (29.5)	1.81 (1.57)	44 (82)
F243T	55	5	42 (90)	26.0 (33.5)	2.97 (1.79)	72 (93)
S101N/F243T	55	5	42 (90)	32.3 (35.3)	3.69 (1.88)	89 (98)
Postconsumer PET waste						
Wild-type	55	5	42 (90)	13.7 (28.2)	1.57 (1.50)	38 (78)
F243T	55	5	42 (90)	28.1 (32.8)	3.21 (1.75)	78 (91)
S101N/F243T	55	5	42 (90)	32.8 (34.9)	3.75 (1.86)	91 (97)
PET microparticles						
Wild-type	72	40	2 (3.5)	19.6 (21.6)	5.88 (3.69)	9.4 (10.4)
T96H	72	40	2 (3.5)	18.3 (21.0)	5.49 (3.60)	8.8 (10.1)
Y127P	72	40	2 (3.5)	20.9 (23.0)	6.27 (3.94)	10 (11)
V212T	72	40	2 (3.5)	16.7 (20.4)	5.01 (3.49)	6.6 (9.8)
F243T	72	40	2 (3.5)	23.2 (24.0)	6.96 (4.11)	11.1 (11.5)
F243T	60	40	2 (3.5)	15.9 (20.2)	4.77 (3.46)	9 (11)
F243T	55	40	2 (3.5)	14.6 (18.4)	4.38 (3.15)	8 (10)
F243T	45	40	2 (3.5)	5.0 (9.8)	1.50 (1.68)	3 (6)
Wild-type	55	5	4 (7.5)	2.9 (3.8)	3.48 (2.43)	2 (2)
F243T	55	5	4 (7.5)	4.3 (5.2)	5.16 (3.33)	2 (3)
S101N/F243T	55	5	4 (7.5)	5.8 (6.2)	6.96 (3.97)	3 (3)

^aInterpolated.; ^bCalculated after 67 h of incubation.

and S101V/F243T) showing a significantly increased activity on PET (from ~ 125% to ~ 184% in comparison to the starting F243T Δ LCC) were selected.

These variants were overexpressed and purified by metal-chelating affinity chromatography using the conditions optimized for the wild-type Δ LCC. The volumetric yield of double variants was significantly increased in comparison to the wild-type protein: a ~ 3.8-fold increase (corresponding to 9.6 mg of protein \cdot L⁻¹ culture) was observed for the A97G/F243T variant (Table S3). Interestingly, and similarly to the F243T variant, the decreased specific activity on *p*NPA (e.g. the S101N/F243T variant showed a specific activity ~ 3-fold lower than the wild-type Δ LCC) was frequently coupled to a significant increase in activity on

PET nanoparticles (Table S3, Fig. 2). In particular, the S101N/F243T and A97T/F243T variants showed the largest increase in activity on PET nanoparticles: ~ 130% and ~ 227% in comparison to the F243T and wild-type Δ LCC.

Kinetics on PET nanoparticles and thermal stability of the Δ LCC variants

A detailed kinetic investigation was performed on wild-type Δ LCC and on the best variants of the first and second round of mutagenesis (i.e. F243T and S101N/F243T, respectively): the turbidity decrease of the PET nanoparticles solution was recorded at increasing enzyme concentrations (up to 60 μ g \cdot mL⁻¹)

(Fig. 4A). The square root of the rate of turbidity decrease, measured in the linear part of the plots, was plotted as a function of the enzyme concentration and data were fitted using (Eqn 1) to obtain the maximal rate of the ester bond cleavage of amorphous PET (k_{τ}) and the affinity constant between the enzyme and PET (K_A). A hyperbolic behaviour was observed for all enzymes (Fig. 4B). The F243T substitution resulted in a significantly improved k_{τ} (134% compared to the wild-type) and in a slightly reduced affinity for PET. The S101N/F243T double variant showed a further increased k_{τ} constant (191% compared to the wild-type) and decreased substrate affinity (K_A was 61% compared to the same value for the wild-type Δ LCC) (Table 3). The effect of TPA on the activity of the

enzyme was investigated up to 35 mM (a close value to the one reached at the end of PET biodegradation experiments): a $22 \pm 1\%$ and $30 \pm 4\%$ inhibition was determined for wild-type and S101N/F243T Δ LCC, respectively, at the maximal product concentration. This result allows to exclude that the improved performance of the double variant is due to a decrease in the product inhibition and that the latter is responsible for the partial PET degradation, as reported in Fig. 3.

The thermal stability of the Δ LCC variants was determined following the loss of secondary structure at increasing temperature by recording the variation of the circular dichroism (CD) signal at 220 nm. Under the experimental conditions employed, the wild-type enzyme possesses a melting temperature (T_m) of

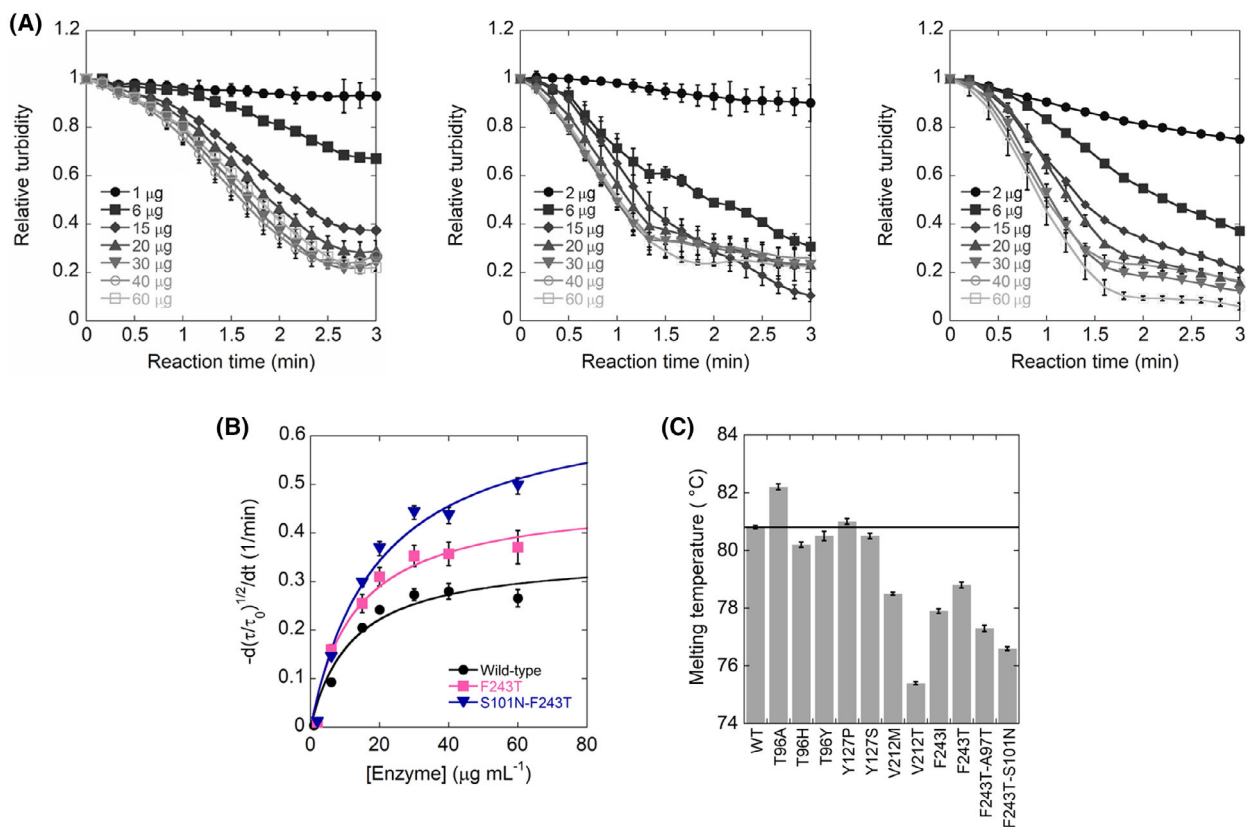


Fig. 4. Kinetic and thermal stability properties of Δ LCC variants. (A) Time course of relative decrease in turbidity of PET nanoparticle solution incubated with increasing concentrations of wild-type (left), F243T (centre), and S101N/F243T (right) Δ LCC variants. Values have been corrected for the control without the enzyme. Values recorded at 10- or 20-s intervals are reported; error bars indicate the standard deviation ($n = 3$). Reaction conditions: $0.094 \text{ mg}\cdot\text{mL}^{-1}$ of nanoparticles in 50 mM Tris-HCl buffer, 100 mM NaCl, pH 8.0, at 50°C with increasing concentrations of Δ LCC variants: 0.001 (●, for Δ LCC) or 0.002 (●, for F243T and S101N/F243T), 0.006 (■), 0.015 (◆), 0.02 (▲), 0.03 (▼), 0.04 (○) and $0.06 \text{ mg}\cdot\text{mL}^{-1}$ (□). (B) Kinetic analysis of Δ LCC variants on PET nanoparticles. Plot of initial depolymerization rates (decrease of the square root of turbidity per minute) determined at increasing concentrations of the Δ LCC variants: wild-type (black), F243T (purple) and S101N/F243T (blue). Experimental data points, shown as circles, were fitted based on Eqn (1). Kinetic measurements were performed in triplicate; conditions as in panel A. (C) Melting temperature of selected Δ LCC variants as determined by loss of protein secondary structure at increasing temperatures followed by CD spectroscopy.

Table 3. Kinetic parameters for the enzymatic hydrolysis of PET nanoparticles by Δ LCC variants at 50 °C (Fig. 4). Data were fitted using (Eqn 1); R^2 is the nonlinear regression coefficient.

Δ LCC variant	k_{τ} (min ⁻¹)	K_A (mL·mg ⁻¹)	R^2
Wild-type	0.355 ± 0.038	83.8 ± 28.4	0.98
F243T	0.475 ± 0.046	78.4 ± 23.0	0.98
S101N/F243T	0.677 ± 0.072	51.3 ± 13.7	0.99

80.8 °C, lower than the value reported in literature (84.7 °C) [23] (Fig. 4C, Table S3). The single point substitutions T96A, T96H, T96Y, Y127P and Y127S did not significantly alter the thermal stability of the enzyme ($\Delta T_m \leq \pm 1.4$ °C). A slight decrease in thermal stability was instead observed for the V212M, F243I and F243T Δ LCC variants (T_m values of 77.9–78.8 °C). The largest decrease in thermal stability was observed for the V212T variant (−5.3 °C compared to the wild-type enzyme, Fig. 4C, Table S3). Concerning the double variants, a further slight decrease in thermal stability (compared to the F243T variant) was observed for the A97T/F243T and S101N/F243T Δ LCC, which showed T_m values of 77.4 °C and 76.6 °C, respectively (Fig. 4C).

Biodegradation of different PET samples by Δ LCC double-point variants

The performance of the two best double variants (S101N/F243T and A97T/F243T Δ LCC) on the amorphous PET film degradation was investigated using the conditions set up for the first-generation variants (i.e. at an incubation temperature lower than the T_g of

PET). At 55 °C, the S101N/F243T variant performed significantly better than the F243T and wild-type Δ LCC (Fig. 5A) while the A97T/F243T variant resembled the F243T. At this temperature, the S101N/F243T Δ LCC hydrolysed 91% of PET film in 65 h (0.31 mmol_{products}·mg_{enzyme}⁻¹·day⁻¹) versus ~68% for the F243T variant. At 60 °C, the rate of hydrolysis was slightly faster in the first part of the bioconversion (0.34 mmol_{products}·mg_{enzyme}⁻¹·day⁻¹ at 39 h), reaching a concentration of products at the end of the bioconversion similar as for reactions at 55 °C (31.3 mM after 70 h, corresponding to an 86% product yield and a hydrolysis rate of 0.27 mmol_{products}·mg_{enzyme}⁻¹·day⁻¹, Fig. 5B). The rate of hydrolysis of the S101N/F243T variant was faster than the one of the A97T/F243T at both temperatures, and 2.0- and 3.5-fold faster than the one of the wild-type Δ LCC at 55 °C and 60 °C respectively (Fig. 5). Notably, the highest yields of PET degradation were observed performing the reaction at the lower temperature (Table 2).

Pilot enzymatic biodegradation reactions of different PET types (amorphous PET film, the reference substrate, and amorphous postconsumer PET) have been set up using the best performing variant (i.e. the S101N/F243T Δ LCC) and at 55 °C, since this temperature represents the best trade-off between reaction rate and depolymerization yield (Table 2). With a view to potential large-scale application of the biocatalyst, the enzyme load was significantly decreased: the highest rate of PET film hydrolysis was observed using an enzyme to PET ratio in the 0.4–1.4 mg_{enzyme}·g_{PET}⁻¹ range (Fig. 6A). At a 0.71 mg_{enzyme}·g_{PET}⁻¹ ratio (5 μ g·mL⁻¹) and 55 °C, the S101N/F243T Δ LCC

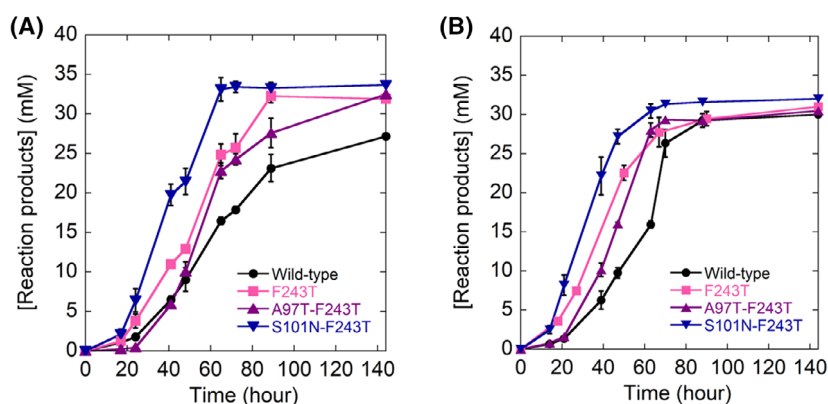


Fig. 5. Biodegradation of amorphous PET film by Δ LCC double variants at (A) 55 °C and (B) 60 °C. The reactions were followed determining the total amount of soluble reaction products in the supernatant of the reaction mixture (continuous line): wild-type (●), F243T (■), A97T/F243T (▲) and S101N/F243T (▼) Δ LCC. The residual activity of the enzyme in solution is reported as dashed lines and open symbols. Error bars indicate the standard deviation ($n = 3$). Reaction conditions: 7 mg·mL⁻¹ of PET film with 0.04 mg·mL⁻¹ of Δ LCC variants in 100 mM potassium phosphate buffer, pH 8.0.

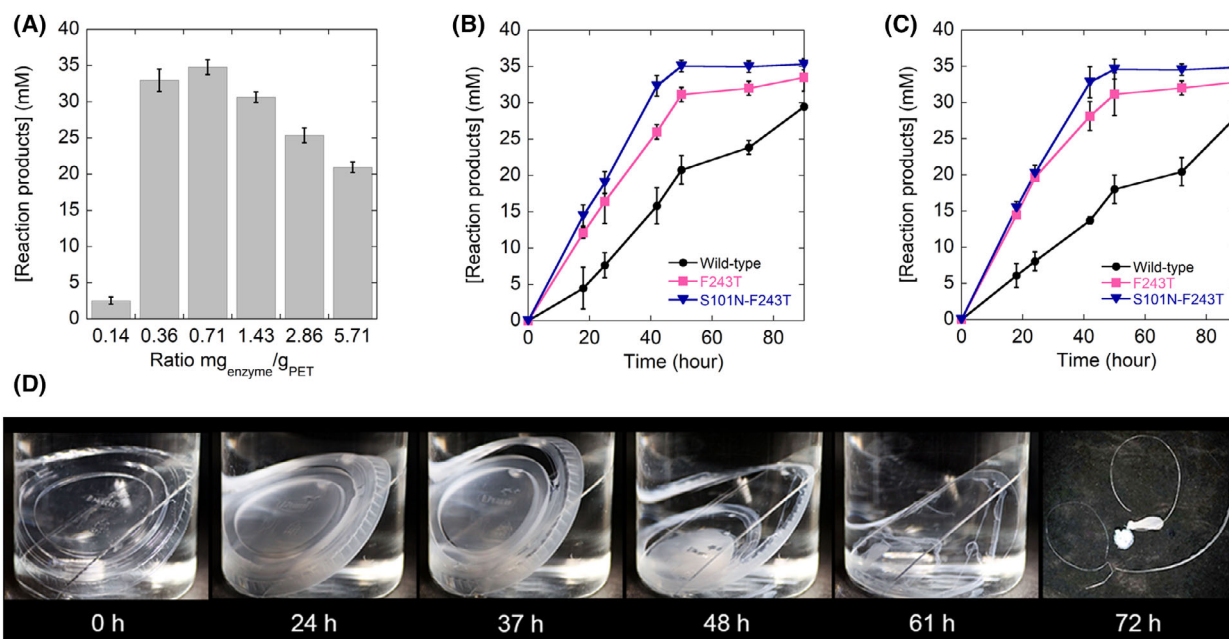


Fig. 6. (A) Biodegradation of amorphous PET film by different concentrations of S101N/F243T Δ LCC. Comparison of biodegradation of 7 mg·mL⁻¹ amorphous PET film with increasing concentration of S101N/F243T Δ LCC from 1 to 40 μ g·mL⁻¹ after 48 h of incubation at 55 °C. Reaction conditions: PET film in 100 mM potassium phosphate buffer, pH 8.0 at 55 °C. Error bars indicate the standard deviation ($n = 3$). Biodegradation of (B) amorphous PET film and (C) postconsumer PET waste by wild-type (●), F243T (■) and S101N/F243T (▼) Δ LCC at 55 °C. The reaction was followed through the determination of the total amount of soluble reaction products in the supernatant of the reaction mixture. Reaction conditions: 7 mg·mL⁻¹ of PET substrates (amorphous PET film or postconsumer PET waste) with 0.005 mg·mL⁻¹ of Δ LCC variants in 100 mM potassium phosphate buffer, pH 8.0. (D) Photoframes of the time-lapse video (Video S1) of the pilot biodegradation of 1.3 g disposable PET jar lid (diameter = 6.5 cm) by S101N/F243T Δ LCC variant at 55 °C in 250 mL of 100 mM potassium phosphate buffer, pH 8.0. In the last photograph of the series, the pieces left over at the end of bioconversion correspond to 0.8% of the starting weight.

performed significantly better than the F243T and wild-type Δ LCC (Fig. 6B,C). At this temperature, the S101N/F243T variant hydrolysed 89% of amorphous PET film and 91% of postconsumer PET waste in 42 h, while at the same time frame the F243T single variant hydrolysed ~72% of amorphous PET film and 78% of postconsumer PET waste. The S101N/F243T Δ LCC was 2.0- and 2.1-fold faster than the wild-type enzyme on the amorphous PET film and postconsumer PET waste substrates, respectively (Fig. 6B,C, Table 2). The use of a lower amount of biocatalyst allowed reaching a productivity rate of 3.69 mmol_{products}·mg_{enzyme}⁻¹·day⁻¹, a value ~12-fold higher than the one obtained using a 5.71 mg_{enzyme}·g_{PET}⁻¹ ratio. The productivity rate for the postconsumer PET waste was even slightly higher (3.75 mmol_{products}·mg_{enzyme}⁻¹·day⁻¹).

Interestingly, 1.25 mg of the S101N/F243T variant fully depolymerized 1.3 g of postconsumer PET waste (disposable PET jar lid, diameter 6.5 cm, 1.2%

crystallinity [17]) in 72 h at 55 °C, with a 99.2% yield (residual PET was 0.01 g) (Fig. 6D, Video S1).

Discussion

In the present study, we applied a semi-rational *in vitro* evolution approach to improve the ability of LCC cutinase to depolymerize the PET polymer. Several single- and double-point variants were produced starting from the Δ LCC wild-type deletion variant. Different biodegradation results were obtained depending on the PET sample used: nanoparticles show a 3000-fold higher surface/mass ratio and a lower crystallinity as compared to microparticles, and PET films are mainly amorphous. These features affect both the affinity of the enzyme for the polymer (and the recognition of attack sites on films) and the enzyme adsorption on the surface, thus altering differently the kinetics and the time course of enzyme inactivation (mostly apparent with PET microparticles).

The best single-point variant (F243T) was able to depolymerize amorphous PET film 1.3-fold better than wild-type Δ LCC enzyme, producing ~ 21.9 mm of soluble products after 27 h of reaction at 72 °C, with a depolymerization rate of $0.49 \text{ mmol}_{\text{product}} \cdot \text{mg}_{\text{enzyme}}^{-1} \cdot \text{day}^{-1}$, and a partial depolymerization ($\sim 67\%$) of PET at the end of the reaction. The low yield was not due to a depletion of the active enzyme from the reaction mixture but to the process of recrystallization of PET at > 70 °C, as previously described [23,28]. The highest PET film depolymerization yield (89%) was observed for the F243T Δ LCC performing the reaction at a lower temperature (55 °C, Fig. 5A). This variant outperformed wild-type Δ LCC also when used to degrade PET microparticles with a very high crystallinity ($> 40\%$). At 72 °C, a depolymerization rate of $\sim 17.4 \text{ mmol}_{\text{product}} \cdot \text{mg}_{\text{enzyme}}^{-1} \cdot \text{day}^{-1}$ was observed (Fig. 3B) with a low overall biodegradation yield ($\sim 12\%$), that confirmed the general difficulty of PHEs to attack the crystalline regions of PET and the necessity of an amorphization treatment prior enzymatic treatment [23].

Focusing on positions 97 and 101, improved double variants were generated starting from the F243T Δ LCC: S101N/F243T and A97T/F243T variants showed the largest increase in activity on PET nanoparticles. A significant increase in k_{τ} for PET nanoparticles at 50 °C was obtained for the S101N/F243T compared to F243T and wild-type Δ LCC (Table 3); this variant also showed a ~ 4 °C lower T_m (Fig. 4C), and a higher ability to degrade amorphous PET (at 55–60 °C, Fig. 5) and postconsumer PET waste (at 55 °C, Fig. 6). From a kinetic point of view, the superior PET degradation performance of the S101N/F243T double variant can be explained based on the Sabatier principle [28]: a substitution that caused the decrease of its affinity for the polymer (from 83.8 to 51.3 $\text{mL} \cdot \text{mg}^{-1}$) resulted into an almost 2-fold increase in the maximal turnover rate (Table 3). This result agrees with the previous observation that the highest turnover rate of LCC was observed in the presence of the surfactant cetyltrimethylammonium bromide (CTAB), causing a 62% decrease in the affinity of the enzyme for PET [30]. This figure exactly corresponds to the decrease in K_A observed for the S101N/F243T Δ LCC (63%). For this reason, we speculate that the changes in PET affinity by the S101N/F243T substitutions allowed Δ LCC to reach the optimal catalytic efficiency.

Analysis of the root mean square fluctuation (RMSF) of the backbone atoms, which is a proxy for protein flexibility, from MD simulations carried out for F243T and S101N/F243T Δ LCC models in

complex with 3PET, suggests that the region of the active site close to position 243 is slightly more flexible in these variants in comparison to the wild-type (Fig. S1B, Fig. 7A). The predicted ΔG_{bind} values ($-36.0 \pm 2.5 \text{ kcal} \cdot \text{mol}^{-1}$ and $\Delta G_{\text{bind}} = -33.3 \pm 1.6 \text{ kcal} \cdot \text{mol}^{-1}$, respectively) are in accordance with the kinetic experiments showing a similar or an almost halved K_A for PET in the case of the single or double variant, respectively (Table 3).

Interestingly, residue F243 of LCC corresponds to residue S238 of PETase from *I. sakaiensis* (Fig. 7B). In the latter PHE, a phenylalanine was previously introduced to narrow the active site by [12], but a subsequent study introducing a smaller alanine resulted in a more active variant [18]. The introduction of an alanine at the same position in IsPETase improved PET binding affinity, especially towards the conformation found in crystalline regions [31], as well as increased 12.7-fold the activity on low crystallinity PET film in the presence of cationic surfactants in *Thermobifida fusca* cutinase TfCut2 (G62A/F209A variant) [32]. The same trend is apparent comparing the two close homologues polyester hydrolases PHL3 and PHL7 [26]. These two enzymes differ only by four residues; in particular, at position 210 (corresponding to position 243 of LCC), PHL3 possesses a phenylalanine while PHL7 (the enzyme showing the best PET hydrolytic activity) holds a smaller leucine residue. Structural analysis allowed to conclude that leucine at position 210 contributed to the high PET hydrolytic activity in PHL7 compared to other PHEs [26]. Altogether, our investigation supports the hypothesis that this specific position at the active site of PHEs, although being ~ 8 Å far away from the active centre Ser165, is a key hotspot for the interaction with PET (Fig. 7C), and the presence of smaller hydrophobic residues resulted in superior activity at the expense of thermostability. On this side, a clear negative correlation exists between the thermal stability of the Δ LCC variants and their activity on PET nanoparticles (Fig. 7D).

Mutagenesis studies have been previously performed also at positions resembling S101 in LCC: in *T. fusca* Tfu_0883 cutinase the substitution of T101 into an alanine, by creating a greater space at the active site, resulted in higher activity on PET [33], while the S93A substitution in IsPETase altered the substrate preference [34].

A straightforward comparison of degradation rates of the S101N/F243T Δ LCC with improved LCC variants reported in literature is not feasible due to different types of substrates and reaction conditions used. Anyway, the S101N/F243T Δ LCC is able to almost fully depolymerize postconsumer PET film ($\sim 90\%$ yield) in < 2 days at a moderate temperature (55 °C)

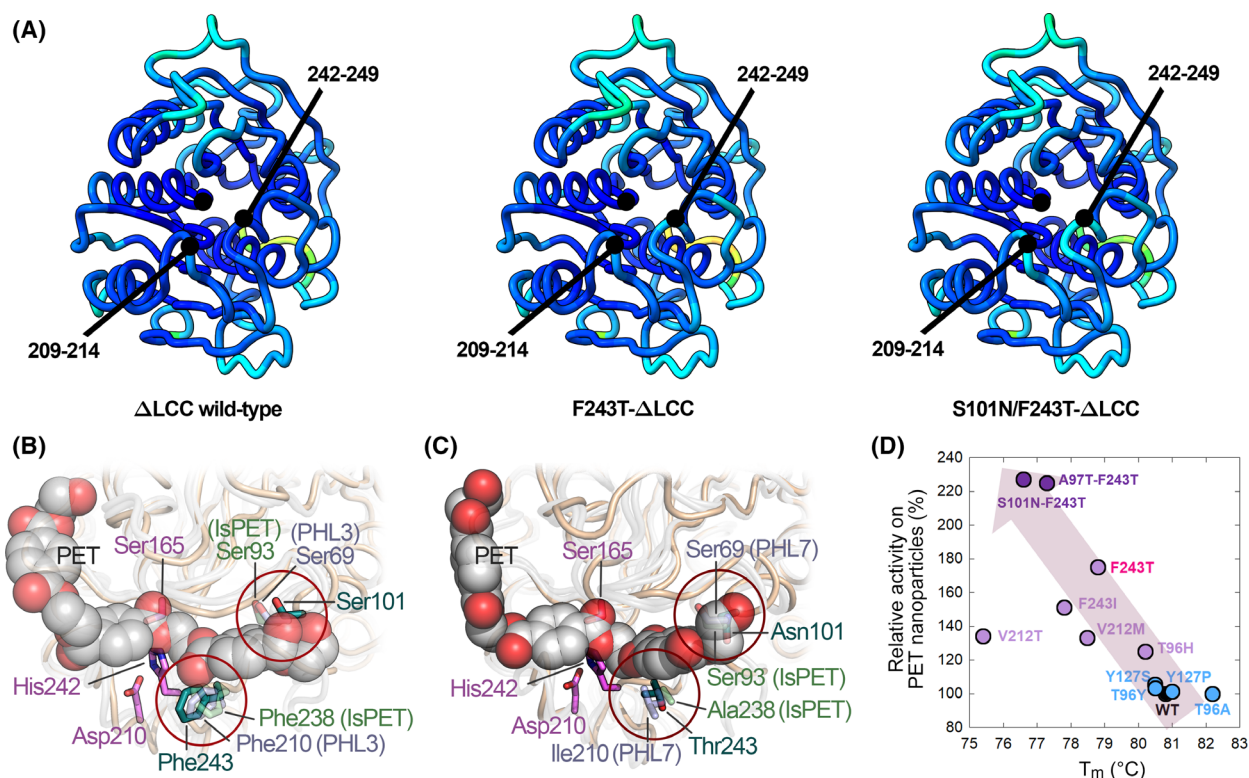


Fig. 7. (A) Per-residue backbone RMSF of MD simulations of wild-type, F243T and F243T/S101N ΔLCC. The backbone of wild-type, F243T and F243T/S101N ΔLCC is represented as ribbon and rainbow coloured according to RMSF values reported above, with increasing values going from blue to red. The black circle indicates the position of the catalytic Ser165. (B) Superimposition of wild-type ΔLCC with docked 3PET, IsPETase from *Ideonella sakaiensis* W159H/S238F variant [12] and PHL3. (C) Superimposition of S101N/F243T ΔLCC variant with docked 3PET, TS-ΔIsPETase variant and PHL7. Residues of LCC are shown in pink (catalytic triad) and in teal (residues 101 and 243); residues of IsPETase are shown in light green; the residues of PHL3 or PHL7 are shown in light purple. The protein backbone of the proteins is shown in wheat (LCC) or in light grey (ΔIsPETase, PHL3 and PHL7). The 3D models of W159H/S238F-IsPETase, S101N/F243T ΔLCC, TS-ΔIsPETase and PHL3 have been produced in PYMOL. Images were prepared with open-source PYMOL 2.5.0 (The PyMOL Molecular Graphics System, Version 2.5.0; Schrödinger, LLC, <https://github.com/schrodinger/pymol-open-source>). PDB code of wild-type ΔLCC and PHL7 are 6EOD and 7NEI respectively. (D) Correlation between the thermal stability (T_m) and the enzymatic activity on PET nanoparticles of the produced ΔLCC variants.

with a depolymerization rate of $3.75 \text{ mmol} \cdot \text{mg}_{\text{enzyme}}^{-1} \cdot \text{day}^{-1}$ (Fig. 6C). This figure is similar to the one reported for the F243I/D238C/S283C/Y127G LCC variant ($4.03 \text{ mmol} \cdot \text{mg}_{\text{enzyme}}^{-1} \cdot \text{day}^{-1}$), a figure obtained at 72°C on pulverized amorphous PET possessing a higher accessible surface area [23]. Furthermore, the PHL7 enzyme depolymerized 17.4 g of post-consumer PET in 2 days at 60°C ($\sim 2.2 \text{ mmol} \cdot \text{mg}_{\text{enzyme}}^{-1} \cdot \text{day}^{-1}$) [26]; our S101N/F243T-ΔLCC variant almost fully depolymerized the same type of substrate showing a similar performance ($\sim 1.8 \text{ mmol} \cdot \text{mg}_{\text{enzyme}}^{-1} \cdot \text{day}^{-1}$) but at a lower temperature (55°C , Fig. 6C).

Most of the protein engineering efforts performed in recent years on PHEs have been aimed at improving the thermal stability of the enzyme, this with the aim

to perform the reaction at high reaction temperatures ($> 70^\circ\text{C}$) [16,23,26,32]. Our findings question the application of this strategy in the case of the thermostable cutinase LCC. Both the wild-type and improved variants of this enzyme can be employed in PET depolymerization at high reaction temperatures (i.e. at 72°C), a condition that favours the conversion of amorphous PET into a more crystalline polymer [23,28], which is almost fully resistant to enzymatic hydrolysis. Consequently, the kinetic competition at 72°C between depolymerization and recrystallization processes prevents reaching a high PET degradation even using a very high enzyme/PET ratio. However, the use at 55°C of the evolved ΔLCC variants reported in the present study allows reaching $\geq 90\%$ depolymerization yield of untreated PET after

≤ 3 days (both amorphous PET and postconsumer PET). From an economic and environmental point of view, the feasibility of performing the whole biodegradation at a lower incubation temperature represents an opportunity to lower the energy demand of the whole PET biocatalytic recycling process, making PET enzymatic degradation an ecofriendly and sustainable process.

Materials and methods

In silico analyses

Docking and molecular dynamics simulations

The PET trimer was prepared and minimized by a steepest-descent algorithm under the general Amber force field (GAFF) by using AVOGADRO 1.2.0 software [35,36]. The AM1-BCC charges were assigned to the ligand by using Antechamber with sqm method in AMBERTOOLS21 package [37,38]. The 3D model of Δ LCC was generated with open-source PYMOL (PyMOL Molecular Graphics System, Version 2.5.0; Schrödinger, LLC, New York, NY, USA, <https://github.com/schrodinger/pymol-open-source>) using the PDB structure of wild-type LCC (PDB ID: 4EB0) [20]. Molecular docking of Δ LCC model with 3PET was carried out with GNINA 1.0 [39]. The box (a square with 20 Å per side) was centred at catalytic Ser165 and an exhaustiveness of 32 was used to sample 10 docking poses with default root-mean-square deviation (RMSD) for clustering. The CNN score was used to rank docking poses. A docking pose was considered catalytically competent if a distance < 4.0 Å was measured between (a) the carbon atom of an ester group and the γ -OH of the catalytic nucleophile Ser165, and (b) the carbonyl oxygen of the same ester group and the N atoms of the backbone of Tyr95 and Met166 (which form the oxyanion hole). This choice was based on previous knowledge of the catalytic mechanism of LCC, the transition state formed in the first reaction step of cutinases [40] and other GxSxG serine-hydrolases [41], and the general rules of nucleophilic biomolecular reactions [42].

The best catalytically competent docking pose was used for further steps. Hydrogens were added to catalytically competent 3PET- Δ LCC docked system with PDB2PQR 3.2.0 [43], according to the predicted pK_a with PROPKA 3.4.0 [44] at pH 8. The hydrogenated system was energetically minimized by using GROMACS 2019.6 [45] (AMBERFF14SB force field [46]), included in a dodecahedron box and solvated in transferable intermolecular potential 3P (TIP3P) water [47] with Na^+ and Cl^- counterions at 100 mM to neutralize the charge. This system was equilibrated under constant pressure and temperature conditions (1 atm and 60 °C) and used as the starting point for three independent 200-ns MD simulations performed while applying an umbrella-

sampling harmonic biasing potential with a null rate and a constant force of $5000 \text{ kJ}\cdot\text{mol}^{-1}\cdot\text{nm}^{-1}$ to restrain ~ 3.5 Å the distance between the carbon of the attacked ester group of 3PET and the γ -OH of the Ser165. This potential was required since the 3PET molecule floated away from the system after ~ 50 ns in its absence, even if a relaxation step of up to 40 ns was applied before to release any potential. The system coordinates were saved every 1 ns. The last 100 ns of each simulation, where the all-atom RMSD was stable, was used for further analyses.

The binding free energy (ΔG_{bind}) of the protein–ligand interaction was estimated by molecular mechanics energies combined with the generalized Born and surface area continuum solvation using MMPBSA.PY [48] from the AMBERTOOLS21 package [49]. The ΔG_{bind} values were averaged over the mean values calculated for each simulation replicate by decomposing their contribution with the per-residue effective free-energy decomposition (prEFED) protocol, as done in [25,50]. Residues were defined as a hot spot of interaction with 3PET if their energy contribution was $\leq -1.0 \text{ kcal}\cdot\text{mol}^{-1}$.

The 3D models of the variants were prepared in CHIMERA 1.16 [51] using the most probable side-chain from the Dunbrack library [52] followed by an energy minimization of the models of the variants.

Predicting the effects due to site-saturation substitutions

The sequence positions predicted to be the hotspot of interaction with the docked substrate were further filtered by considering the average relative variation (%) of the sequence Hamiltonian upon all other 19-point mutations (relaxation enthalpy, ΔH_{rel}). ΔH_{rel} was used as a predictor of the changes of protein function or stability at each site, with more negative values related to sites for which SSM is expected to produce a lower amount of stable and functional variants, as proposed by [53]. ΔH_{rel} for each Δ LCC amino acid was calculated by using the EV-couplings package (<https://github.com/debbiemarkslab/EVcouplings>, [54]) after fitting a Potts model to an alignment representative of the cutinase family with PLMC package (<https://github.com/debbiemarkslab/plmc>, [55]). Three analyses were performed with different values for the θ parameter (0, 0.2, 0.3), which controls the relative pairwise sequence difference that is used as a threshold to down weight similar sequences. ΔH_{rel} values were then averaged over these replicates. The multiple sequence alignment was obtained by using the sequence of Δ LCC as query for a MMseq2 (release 13–45 111) search [56,57] on ColabFold clustered UniRef100 and BFD/MGnify databases (<https://colabfold.mmseqs.com/>). The resulting 7503 aligned sequences were checked for the presence of the catalytic triad, clustered at max 95% identity and sequences showing $< 75\%$ alignment coverage were discarded, with HHBLITS 3.3.0 [58], resulting in a final alignment of 2840 sequences. Sites were

considered good candidates for SSM when the ΔH_{rel} (0-averaged) was higher than the average ΔH_{rel} (0-averaged) over the full sequence (i.e. > -0.571).

Preparation of PET nanoparticles

Poly(ethylene terephthalate) nanoparticles were prepared from PET microplastic (diameter 300 μm ; Goodfellow GmbH, Bad Nauheim, Germany) using a precipitation and solvent evaporation technique [18,27]. PET nanoparticles showed a mean diameter of 80 nm (as determined by dynamic light scattering) and a concentration of $630 \pm 80 \mu\text{g}\cdot\text{mL}^{-1}$ [18].

Cloning, expression and purification of ΔLCC

The synthetic gene encoding ΔLCC (optimized for *Escherichia coli* heterologous expression) was synthesized by GeneArt (Thermo Fisher Scientific, Waltham, MA, USA) based on the UniProt G9BY57 protein sequence. The nucleotide sequence coding for the 34-residue-long N-terminal secretion sequence was removed from the synthetic DNA by mutagenic polymerase chain reaction (PCR) (Fig. S2).

The PCR product was subcloned into the pET24b expression vector with *NdeI* and *XhoI* restriction enzymes; the resulting plasmid was transformed into the Origami2 (DE3) *E. coli* strain. The recombinant protein was expressed in 1 L of Luria–Bertani broth medium containing $5 \mu\text{g}\cdot\text{mL}^{-1}$ tetracycline and $30 \mu\text{g}\cdot\text{mL}^{-1}$ kanamycin at 37°C . After induction of protein expression by adding 0.1 mM isopropyl β -D-1-thiogalactopyranoside, the culture was incubated for 16 h at 17°C . The cells were harvested by centrifugation and lysed by sonication in lysis buffer (50 mM Tris–HCl, pH 8.0, 500 mM NaCl, 20 mM imidazole, 1 mM pepstatin, $10 \mu\text{g}\cdot\text{mL}^{-1}$ DNase). After centrifugation at 39 000 *g* for 45 min at 4°C , the crude extract was loaded onto a 1-mL HiTrap chelating column (GE Healthcare, Chicago, IL, USA) equilibrated in binding buffer (50 mM Tris–HCl, 500 mM NaCl, 20 mM imidazole, pH 8.0). ΔLCC was eluted with 50 mM Tris–HCl, 200 mM NaCl, 500 mM imidazole (pH 8.0) and equilibrated in 25 mM Tris–HCl, 200 mM NaCl (pH 8.0) by size-exclusion chromatography using a PD-10 desalting column (GE Healthcare). ΔLCC concentration was estimated based on the theoretical extinction coefficient at 280 nm of $38\,453 \text{ M}^{-1}\cdot\text{cm}^{-1}$. The same protocol was used to express and purify ΔLCC variants generated by SSM.

Site-saturation mutagenesis reactions and production of mutant libraries

Site-directed mutagenesis was carried out at positions 95, 96, 127, 166, 212 and 243 using the QuickChange II XL

Site-Direct Mutagenesis kit (Agilent Technologies, Santa Clara, CA, USA), the gene encoding ΔLCC as template and the primers carrying NNK-degenerated codons at the desired positions (i.e. degenerated primers with N = A, C, G, or T and K = G or T, Table S2). The amplification mixture was used to transform *E. coli* NEB 10- β cells obtaining libraries of approximately 3000 clones each. SSM was also carried out at positions 97 and 101 using the gene encoding F243T ΔLCC as template.

High-throughput screening for evolved ΔLCC variants

The plasmid DNA pools containing the whole genetic variability generated by SSM were transferred to the Origami2 (DE3) *E. coli* expression strain for the enzymatic activity screening, based on a colorimetric assay with phenolsulfonphthalein dye (PSP, Phenol Red dye) and using of the epMotion 5075 automated liquid-handler system (Eppendorf, Hamburg, Germany) [27]. A 0.1 mM final concentration of IPTG was added to 1 mL *E. coli* cultures grown at saturation in deepwell plates at 37°C and the cells were incubated at 17°C for 16 h. 0.9 mL of each culture was centrifuged, and the pellet was resuspended with 0.4 mL of lysis solution (1 mM sodium phosphate buffer, pH 8.1, 100 mM NaCl, $40 \mu\text{g}\cdot\text{mL}^{-1}$ lysozyme) for 30 min at 37°C . The crude extract (0.1 mL) was transferred into a well of a 96-well plate. The hydrolytic activity was assayed by adding 3 mM BHET or 0.21 mg of PET nanoparticles and 0.2 mM PSP. After incubation at 50°C for 3 h, the absorbance at 540 nm was recorded by a microtitre plate reader (Infinite 200; Tecan, Männedorf, Switzerland) and compared with the figure for cells expressing the ΔLCC (positive control) and cells transformed with pET24b empty vector (negative control). Clones showing an increased activity were confirmed by a second screening and the gene coding for the variant was sequenced.

Activity assay

The reference hydrolytic enzymatic activity on 1 mM *p*-nitrophenyl acetate (*p*NPA) was measured by recording the absorbance increase due to the product *p*-nitrophenolate at 405 nm ($\epsilon_{405} = 11.6 \text{ mM}^{-1}\cdot\text{cm}^{-1}$) [59]. The reaction was performed at 30°C in 25 mM Tris–HCl, 200 mM NaCl (pH 8.0).

Activity on PET nanoparticles was measured by a turbidimetric assay. PET nanoparticles ($\sim 94 \mu\text{g}\cdot\text{mL}^{-1}$) were incubated in 25 mM Tris–HCl, 200 mM NaCl (pH 8.0), at 50°C with $20 \mu\text{g}\cdot\text{mL}^{-1}$ enzyme; the reaction mixture was mixed by inversion and incubated for 10 min in a cuvette. The turbidity (OD_{600}) was measured every 10 s using a Jasco V-560 spectrophotometer (Jasco Inc., Easton, MD, USA). The relative turbidity τ/τ_0 was calculated as reported

in Refs [18,27]. The kinetic parameters for the heterogeneous enzymatic hydrolysis of PET were determined using the turbidimetric assay at increasing concentrations of enzyme (up to 60 $\mu\text{g}\cdot\text{mL}^{-1}$) and applying a kinetic model of heterogeneous biocatalysis [60,61]. The following Eqn (1) was used to fit the kinetic data [62]:

$$-\frac{d\left(\frac{x}{x_0}\right)^{\frac{1}{2}}}{dt} = \frac{k_{\tau} \cdot K_A \cdot [E]}{1 + K_A \cdot [E]} \quad (1)$$

where $-d(\tau/x_0)^{1/2}/dt$ is the initial rate of the square root of the relative turbidity decrease in the linear region, K_A is the adsorption equilibrium constant, and k_{τ} is the relative maximum rate for cleavage of the ester bond of PET. Values of $-d(\tau/x_0)^{1/2}/dt$ are expected to be linearly dependent on the concentration of PET nanoparticles at a constant enzyme concentration only whether the amount of substrate has saturated the enzyme [27].

Thermal stability of ΔLCC variants

The melting temperature (T_m) for secondary structure of ΔLCC variants was determined by measuring the variation in ellipticity signal by circular dichroism at 222 nm during temperature ramps [63]. Proteins (0.1 $\text{mg}\cdot\text{mL}^{-1}$) were dissolved in 25 mM Tris-HCl, 200 mM NaCl (pH 8.0).

Enzymatic bioconversion of PET

Poly(ethylene terephthalate) film was cut into dishes of 6 mm of diameter (corresponding to ~ 7 mg) and washed with 0.1% SDS, ethanol and deionized water, followed by drying at 50 $^{\circ}\text{C}$ for 1 h. ΔLCC variants (40 $\mu\text{g}\cdot\text{mL}^{-1}$) were added to 1.0 mL of 7 $\text{mg}\cdot\text{mL}^{-1}$ of PET film (Goodfellow Cambridge Ltd., Huntingdon, UK, 250 μm thick, amorphous, product number ES301445) or 40 $\text{mg}\cdot\text{mL}^{-1}$ of PET microplastic (Goodfellow Cambridge Ltd., diameter 300 μm , crystallinity > 40%, product number ES306030) in 100 mM potassium phosphate, pH 8.0 at 45 $^{\circ}\text{C}$, 55 $^{\circ}\text{C}$, 60 $^{\circ}\text{C}$, or 72 $^{\circ}\text{C}$.

A transparent and untreated postconsumer PET waste (bean cake plastic container, 1.2% crystallinity) [17] was cut into dishes of 6 mm of diameter (corresponding to ~ 7 mg) and washed as above. ΔLCC variants (0.005 $\text{mg}\cdot\text{mL}^{-1}$) were added to 1.0 mL of 7 $\text{mg}\cdot\text{mL}^{-1}$ of PET substrate in 100 mM potassium phosphate, pH 8.0 at 55 $^{\circ}\text{C}$.

The concentration of the soluble aromatic products possessing C=O bonds (e.g. MHET, TPA and BHET) was determined from the absorbance at 240 nm ($\epsilon_{240} = 13.8 \text{ mm}^{-1}\cdot\text{cm}^{-1}$) [18]. The residual activity of ΔLCC variants was determined by the *p*NPA assay as described above.

An untreated and transparent postconsumer PET waste (1.3 g, disposable PET jar lid, diameter 6.5 cm) was added to 0.005 $\text{mg}\cdot\text{mL}^{-1}$ of S101N/F243T ΔLCC in 0.25 L of 100 mM potassium phosphate, pH 8.0 at 55 $^{\circ}\text{C}$ for 72 h.

Acknowledgments

The authors thank Davide Tessaro (Politecnico di Milano) for PET nanoparticles preparation. This research was funded by Ministero dell'Universita' and Consorzio Interuniversitario per le Biotecnologie CIB - "Sviluppo catalisi dell'innovazione nelle biotecnologie", MIUR-ex-D.M.-738-(8/8/2019) (LP and GM), Project PRIN2020 - aN InseCt bioEactor for the full valorization of PolyEthylene Terephthalate (NICE-PET) grant number 2020ENH3NZ (GM), Universita' degli Studi dell'Insubria - Fondo di Ateneo per la Ricerca (2019) (LP and GM). MO was supported by a post-doc research fellow (Universita' degli Studi dell'Insubria - Assegno di Ricerca Junior 2019) of the University of Insubria and VP was supported by Consorzio Interuniversitario Reattivita' Chimica e Catalisi - CIRCC "Progetto Competitivo 2020" CMPT200224 (2021). CB is a student of the "Life Sciences and Biotechnology" course at the University of Insubria. Open Access Funding provided by Universita' degli Studi dell'Insubria within the CRUI-CARE Agreement.

Conflict of interest

The authors declare no conflict of interest.

Author contributions

VP performed the experiments, MO performed the bioinformatics analysis, CB performed the kinetic analysis, LP critically read the manuscript and edited manuscript, and GM planned and supervised the work and wrote the main manuscript text. All authors have read and agreed to the published version of the manuscript.

Peer review

The peer review history for this article is available at <https://publons.com/publon/10.1111/febs.16736>.

Data availability statement

The data that support the findings of this study are available in Figs 1–7, Tables 1–3 and the [Supporting Information](#) of this article.

References

- Geyer R, Jambeck JR & Law KL (2017) Production, use, and fate of all plastics ever made. *Sci Adv* **3**, 25–29.

- 2 PlasticsEurope AISBL (2018) *Plastics – The Facts 2018: An Analysis of European Plastics Production, Demand and Waste Data*. PlasticsEurope AISBL, Brussels.
- 3 Leslie HA, van Velzen MJM, Brandsma SH, Vethaak AD, Garcia-Vallejo JJ & Lamoree MH (2022) Discovery and quantification of plastic particle pollution in human blood. *Environ Int* **163**, 107199.
- 4 Jenner LC, Rotchell JM, Bennett RT, Cowen M, Tentzeris V & Sadofsky LR (2022) Detection of microplastics in human lung tissue using μ FTIR spectroscopy. *Sci Total Environ* **831**, 154907.
- 5 Cverenkárová K, Valachovičová M, Mackulák T, Žemlička L & Bírošová L (2021) Microplastics in the food chain. *Life* **11**, 1349.
- 6 Pirillo V & Baranzini N (2022) Current research on the effects of plastics pollution in marine and freshwater aquatic invertebrates. *Invertebr Surviv J* **19**, 136–149.
- 7 Webb HK, Arnott J, Crawford RJ & Ivanova EP (2013) Plastic degradation and its environmental implications with special reference to poly(ethylene terephthalate). *Polymers* **5**, 1–18.
- 8 Kim HT, Kim JK, Cha HG, Kang MJ, Lee HS, Khang TU, Yun EJ, Lee D-H, Song BK, Park SJ *et al.* (2019) Biological valorization of poly(ethylene terephthalate) monomers for upcycling waste PET. *ACS Sustain Chem Eng* **7**, 19396–19406.
- 9 Magalhães RP, Cunha JM & Sousa SF (2021) Perspectives on the role of enzymatic biocatalysis for the degradation of plastic PET. *Int J Mol Sci* **22**, 11257.
- 10 Yoshida S, Hiraga K, Takanaha T, Taniguchi I, Yamaji H, Maeda Y, Toyohara K, Miyamoto K, Kimura Y & Oda K (2016) A bacterium that degrades and assimilates poly(ethyleneterephthalate). *Science* **351**, 1196–1199.
- 11 Han X, Liu W, Huang JW, Ma J, Zheng Y, Ko TP, Xu L, Cheng YS, Chen CC & Guo RT (2017) Structural insight into catalytic mechanism of PET hydrolase. *Nat Commun* **8**, 1–6.
- 12 Austin HP, Allen MD, Donohoe BS, Rorrer NA, Kearns FL, Silveira RL, Pollard BC, Dominick G, Duman R, El Omari K *et al.* (2018) Characterization and engineering of a plastic-degrading aromatic polyesterase. *Proc Natl Acad Sci USA* **115**, E4350–E4357.
- 13 Palm GJ, Reisky L, Böttcher D, Müller H, Michels EAP, Walczak MC, Berndt L, Weiss MS, Bornscheuer UT & Weber G (2019) Structure of the plastic-degrading *Ideonella sakaiensis* MHETase bound to a substrate. *Nat Commun* **10**, 1–10.
- 14 Barth M, Honak A, Oeser T, Wei R, Belisário-Ferrari MR, Then J, Schmidt J & Zimmermann W (2016) A dual enzyme system composed of a polyester hydrolase and a carboxylesterase enhances the biocatalytic degradation of polyethylene terephthalate films. *Biotechnol J* **11**, 1082–1087.
- 15 Wei R & Zimmermann W (2017) Microbial enzymes for the recycling of recalcitrant petroleum-based plastics: how far are we? *J Microbial Biotechnol* **10**, 1308–1322.
- 16 Cui Y, Chen Y, Liu X, Dong S, Tian Y, Qiao Y, Mitra R, Han J, Li C, Han X *et al.* (2021) Computational redesign of a PETase for plastic biodegradation under ambient condition by the GRAPE strategy. *ACS Catal* **11**, 1340–1350.
- 17 Lu H, Diaz DJ, Czarnecki NJ, Zhu C, Kim W, Shroff R, Acosta DJ, Alexander BR, Cole HO, Zhang Y *et al.* (2022) Machine learning-aided engineering of hydrolases for PET depolymerization. *Nature* **604**, 662–667.
- 18 Pirillo V, Orlando M, Tessaro D, Pollegioni L & Molla G (2022) An efficient protein evolution workflow for the improvement of bacterial PET hydrolyzing enzymes. *Int J Mol Sci* **23**, 264.
- 19 Son HF, Cho IJ, Joo S, Seo H, Sagong HY, Choi SY, Lee SY & Kim KJ (2019) Rational protein engineering of thermo-stable PETase from *Ideonella sakaiensis* for highly efficient PET degradation. *ACS Catal* **9**, 3519–3526.
- 20 Sulaiman S, Yamato S, Kanaya E, Kim J-J, Koga Y, Takano K & Kanaya S (2012) Isolation of a novel cutinase homologue with polyethylene terephthalate-degrading activity from leaf-branch compost by using a metagenomic approach. *Appl Environ Microbiol* **78**, 1556–1562.
- 21 Sulaiman S, You D-J, Kanaya E, Koga Y & Kanaya S (2014) Crystal structure and thermodynamic and kinetic stability of metagenome-derived LC-Cutinase. *Biochemistry* **53**, 1858–1869.
- 22 Shirke AN, White C, Englaender JA, Zwarycz A, Butterfoss GL, Linhardt RJ & Gross RA (2018) Stabilizing leaf and branch compost cutinase (LCC) with glycosylation: mechanism and effect on PET hydrolysis. *Biochemistry* **57**, 1190–1200.
- 23 Tournier V, Topham CM, Gilles A, David B, Folgoas C, Moya-Leclair E, Kamionka E, Desrousseaux ML, Texier H, Gavalda S *et al.* (2020) An engineered PET depolymerase to break down and recycle plastic bottles. *Nature* **580**, 216–219.
- 24 Niemeyer M, Moreno Castillo E, Ihling CH, Iacobucci C, Wilde V, Hellmuth A, Hoehenwarter W, Samodelov SL, Zurbriggen MD, Kastiris PL *et al.* (2020) Flexibility of intrinsically disordered degrons in AUX/IAA proteins reinforces auxin co-receptor assemblies. *Nat Commun* **11**, 1–18.
- 25 Ubbiali D, Orlando M, Kovačič M, Iacobucci C, Semrau MS, Bajc G, Fortuna S, Ilc G, Medagli B, Oloketuyi S *et al.* (2021) An anti-HER2 nanobody binds to its antigen HER2 via two independent paratopes. *Int J Biol Macromol* **182**, 502–511.
- 26 Sonnendecker C, Oeser J, Richter PK, Hille P, Zhao Z, Fischer C, Lippold H, Blázquez-Sánchez P, Engelberger F, Ramírez-Sarmiento CA *et al.* (2022) Low carbon footprint recycling of post-consumer PET plastic with a

- metagenomic polyester hydrolase. *ChemSusChem* **15**, e202101062.
- 27 Pirillo V, Pollegioni L & Molla G (2021) Analytical methods for the investigation of enzyme-catalysed degradation of polyethylene terephthalate. *FEBS J* **288**, 4730–4745.
- 28 Thomsen TB, Hunt CJ & Meyer AS (2022) Influence of substrate crystallinity and glass transition temperature on enzymatic degradation of polyethylene terephthalate (PET). *N Biotechnol* **69**, 28–35.
- 29 Tarazona NA, Wei R, Brott S, Pfaff L, Bornscheuer UT, Lendlein A & Machatschek R (2022) Rapid depolymerization of poly(ethylene terephthalate) thin films by a dual-enzyme system and its impact on material properties. *Chem Catal* **2**, 3573–3589.
- 30 Baath JA, Jensen K, Borch K, Westh P & Kari J (2022) Sabatier principle for rationalizing enzymatic hydrolysis of a synthetic polyester. *J Am Chem Soc* **2**, 1223–1231.
- 31 Guo B, Vanga SR, Lopez-Lorenzo X, Saenz-Mendez P, Rönnblad Ericsson S, Fang Y, Ye X, Schriever K, Bäckström E, Biundo A *et al.* (2022) Conformational selection in biocatalytic plastic degradation by PETase. *ACS Catal* **12**, 3397–3409.
- 32 Furukawa M, Kawakami N, Tomizawa A & Miyamoto K (2019) Efficient degradation of poly(ethylene terephthalate) with *Thermobifida fusca* cutinase exhibiting improved catalytic activity generated using mutagenesis and additive-based approaches. *Sci Rep* **9**, 16038.
- 33 Silva C, Da S, Silva N, Matamá T, Araújo R, Martins M, Chen S, Chen J, Wu J, Casal M *et al.* (2011) Engineered *Thermobifida fusca* cutinase with increased activity on polyester substrates. *Biotechnol J* **6**, 1230–1239.
- 34 Liu C, Shi C, Zhu S, Wei R & Yin CC (2019) Structural and functional characterization of polyethylene terephthalate hydrolase from *Ideonella sakaiensis*. *Biochem Biophys Res Commun* **508**, 289–294.
- 35 Wang J, Wolf RM, Caldwell JW, Kollman PA & Case DA (2004) Development and testing of a general Amber force field. *J Comput Chem* **25**, 1157–1174.
- 36 Hanwell MD, Curtis DE, Lonie DC, Vandermeersch T, Zurek E & Hutchison GR (2012) Avogadro: an advanced semantic chemical editor, visualization, and analysis platform. *J Cheminform* **4**, 1–17.
- 37 Jakalian A, Jack DB & Bayly CI (2002) Fast, efficient generation of high-quality atomic charges. AM1-BCC model: II. Parameterization and validation. *J Comput Chem* **23**, 1623–1641.
- 38 Salomon-Ferrer R, Götz AW, Poole D, le Grand S & Walker RC (2013) Routine microsecond molecular dynamics simulations with AMBER on GPUs. 2. Explicit solvent particle mesh Ewald. *J Chem Theory Comput* **9**, 3878–3888.
- 39 McNutt AT, Francoeur P, Aggarwal R, Masuda T, Meli R, Ragoza M, Sunseri J & Koes DR (2021) GNINA 1.0: molecular docking with deep learning. *J Cheminform* **13**, 1–20.
- 40 Longhi S & Cambillau C (1999) Structure–activity of cutinase, a small lipolytic enzyme. *Biochim Biophys Acta* **1441**, 185–196.
- 41 Oh C, Doohun Kim T & Kim KK (2019) Carboxylic ester hydrolases in bacteria: active site, structure, function and application. *Crystals* **9**, 597.
- 42 Sadiq SK & Coveney PV (2015) Computing the role of near attack conformations in an enzyme-catalysed nucleophilic bimolecular reaction. *J Chem Theory Comput* **11**, 316–324.
- 43 Dolinsky TJ, Czodrowski P, Li H, Nielsen JE, Jensen JH, Klebe G & Baker NA (2007) PDB2PQR: expanding and upgrading automated preparation of biomolecular structures for molecular simulations. *Nucleic Acids Res* **35**, W522–W525.
- 44 Olsson MHM, Søndergaard CR, Rostkowski M & Jensen JH (2011) PROPKA3: consistent treatment of internal and surface residues in empirical pK_a predictions. *J Chem Theory Comput* **7**, 525–537.
- 45 Abraham MJ, Murtola T, Schulz R, Páll S, Smith JC, Hess B & Lindahl E (2015) Gromacs: high performance molecular simulations through multi-level parallelism from laptops to supercomputers. *SoftwareX* **1–2**, 19–25.
- 46 Maier JA, Martinez C, Kasavajhala K, Wickstrom L, Hauser KE & Simmerling C (2015) ff14SB: improving the accuracy of protein side chain and backbone parameters from ff99SB. *J Chem Theory Comput* **11**, 3696–3713.
- 47 Jorgensen WL, Chandrasekhar J, Madura JD, Impey RW & Klein ML (1983) Comparison of simple potential functions for simulating liquid water. *J Chem Phys* **79**, 926–935.
- 48 Miller BR, McGee TD, Swails JM, Homeyer N, Gohlke H & Roitberg AE (2012) MMPBSA.py: an efficient program for end-state free energy calculations. *J Chem Theory Comput* **8**, 3314–3321.
- 49 Sun H, Li Y, Tian S, Xu L & Hou T (2014) Assessing the performance of MM/PBSA and MM/GBSA methods. 4. Accuracies of MM/PBSA and MM/GBSA methodologies evaluated by various simulation protocols using PDBbind data set. *Phys Chem Chem Phys* **16**, 16719–16729.
- 50 Orlando M, Fortuna S, Oloketuyi S, Bajc G, Goldenzweig A & de Marco A (2021) CDR1 composition can affect nanobody recombinant expression yields. *Biomolecules* **11**, 1362.
- 51 Pettersen EF, Goddard TD, Huang CC, Couch GS, Greenblatt DM, Meng EC & Ferrin TE (2004) UCSF Chimera – a visualization system for exploratory research and analysis. *J Comput Chem* **25**, 1605–1612.
- 52 Shapovalov MV & Dunbrack RL (2011) A smoothed backbone-dependent rotamer library for proteins derived from adaptive kernel density estimates and regressions. *Structure* **19**, 844–858.

- 53 Chi H, Zhou Q, Tutol JN, Phelps SM, Lee J, Kapadia P, Morcos F & Dodani SC (2022) Coupling a live cell directed evolution assay with coevolutionary landscapes to engineer an improved fluorescent rhodopsin chloride sensor. *ACS Synth Biol* **11**, 1627–1638.
- 54 Hopf TA, Green AG, Schubert B, Mersmann S, Schärfe CPI, Ingraham JB, Toth-Petroczy A, Brock K, Riesselman AJ, Palmedo P *et al.* (2019) The EVcouplings Python framework for coevolutionary sequence analysis. *Bioinformatics* **35**, 1582–1584.
- 55 Hopf TA, Ingraham JB, Poelwijk FJ, Schärfe CPI, Springer M, Sander C & Marks DS (2017) Mutation effects predicted from sequence co-variation. *Nat Biotechnol* **35**, 128–135.
- 56 Mirdita M, von den Driesch L, Galiez C, Martin MJ, Söding J & Steinegger M (2017) Uniclust databases of clustered and deeply annotated protein sequences and alignments. *Nucleic Acids Res* **45**, D170–D176.
- 57 Mirdita M, Steinegger M & Söding J (2019) MMseqs2 desktop and local web server app for fast, interactive sequence searches. *Bioinformatics* **35**, 2856–2858.
- 58 Remmert M, Biegert A, Hauser A & Söding J (2012) HHblits: lightning-fast iterative protein sequence searching by HMM-HMM alignment. *Nat Methods* **9**, 173–175.
- 59 Sehata S, Suzuki R & Koumoto K (2017) Increased yield of B-glucosidase-catalysed hydrolysis reactions in the presence of betaine-type metabolite analog. *Bioprocess Biosyst Eng* **40**, 153–159.
- 60 Scandola M, Focarete ML & Frisoni G (1998) Simple kinetic model for the heterogeneous enzymatic hydrolysis of natural poly(3-hydroxybutyrate). *Macromolecules* **31**, 3846–3851.
- 61 Herzog K, Müller RJ & Deckwer WD (2006) Mechanism and kinetics of the enzymatic hydrolysis of polyester nanoparticles by lipases. *Polym Degrad Stab* **91**, 2486–2498.
- 62 Wei R, Oeser T, Barth M, Weigl N, Lübs A, Schulz-Siegmund M, Hacker MC & Zimmermann W (2014) Turbidimetric analysis of the enzymatic hydrolysis of polyethylene terephthalate nanoparticles. *J Mol Catal B Enzym* **103**, 72–78.
- 63 Caldinelli L, Molla G, Bracci L, Lelli B, Pileri S, Cappelletti P, Sacchi S & Pollegioni L (2010) Effect of ligand binding on human D-amino acid oxidase: implications for the development of new drugs for schizophrenia treatment. *Protein Sci* **19**, 1500–1512.

Supporting information

Additional supporting information may be found online in the Supporting Information section at the end of the article.

Fig. S1. MD simulation of Δ LCC.

Fig. S2. Nucleotide and amino acid sequence optimized for expression in *E. coli* of the synthetic DNA fragment encoding the Δ LCC.

Fig. S3. Biodegradation of 7 mg mL^{-1} of amorphous PET film catalysed by F243T Δ LCC variant at 45°C for 400 h.

Table S1. List of the NNK primers used for site-saturation mutagenesis reactions of Δ LCC.

Table S2. Variants of Δ LCC identified at positions 95, 96, 127, 166, 212, 243 (first generation) and at positions 97 and 101 (second generation) for possessing increased activity on PET nanoparticles.

Table S3. Production yield, specific activity on *p*NPA, relative activity on PET nanoparticles and thermal stability of wild-type Δ LCC and selected variants.

Video S1. Time-lapse of biodegradation of a 1.3 g disposable PET jar lid by S101N/F243T Δ LCC variant at 55°C .